Chemical Engineering Journal 442 (2022) 136306

Contents lists available at ScienceDirect

Chemical Engineering Journal

journal homepage: www.elsevier.com/locate/cej

Ag(I) removal and recovery from wastewater adopting NH_2-MIL-125 as efficient adsorbent: A 3Rs (reduce, recycle and reuse) approach and practice

Xueying Ren [a,b], Chong-Chen Wang [a,b,*], Yang Li [a], Chao-Yang Wang [a], Peng Wang [a], Shijie Gao [a]

[a] Beijing Key Laboratory of Functional Materials for Building Structure and Environment Remediation, Beijing University of Civil Engineering and Architecture, Beijing 100044, China

[b] Beijing Energy Conservation & Sustainable Urban and Rural Development Provincial and Ministry Co-construction Collaboration Innovation Center, Beijing University of Civil Engineering and Architecture, Beijing 100044, China

ARTICLE INFO

Keywords:
NH_2-MIL-125
Silver ion
Adsorption
Mechanism
3Rs approach

ABSTRACT

In this work, NH_2-MIL-125(Ti) were adopted to eliminate Ag(I) from the simulated silver-plating wastewater. The results revealed that NH_2-MIL-125 exhibited superior adsorption performance toward Ag(I) ions with uptake capacity of 192.5 $mg{\cdot}g^{-1}$ to that of MIL-125 (139.8 $mg{\cdot}g^{-1}$) within 60 min. The isotherm and kinetic data were exactly fitted to both Langmuir and Pseudo-second-order models. The thermodynamic parameters like enthalpy change (ΔH^o), entropy change (ΔS^o) and Gibbs free energy change (ΔG^o) confirmed that the adsorption process was spontaneous, exothermic and disordered. As well, the influencing parameters of the adsorption process like pH, adsorbent dose and foreign metal ions were examined. The fixed-bed column filled with NH_2-MIL-125 powder immobilized onto cotton fiber could continuously adsorb Ag(I), which offered the possibility of achieving potential large-scale applications. The possible adsorption mechanism of NH_2-MIL-125 toward Ag(I) primarily involved the electrostatic adsorption and coordinative interactions, which was further affirmed by the density functional theory (DFT) calculations. In addition, the used NH_2-MIL-125 saturated with Ag(I) ions could be either desorbed to release the Ag(I) for NH_2-MIL-125 re-generation or further calcinated into Ag/C/TiO_2 photocatalyst to accomplish photocatalytic degradation toward organic pollutants like methylene blue (MB) and phenol. In this work, the 3Rs (reduce, recycle and reuse) approach was practiced, accomplishing that one stone killed three birds (pollutant elimination, resource recovery and resource utilization).

1. Introduction

Various heavy metal ions like silver, copper and zinc existed in the silver plating wastewater, which might interact with the anionic ligands to form complexes or chelates in water to enhance their biotoxicity [1]. Also, the heavy metal ions sunk in the water body might be available by the human body via the food chain, which might exert serious threat to the human health [2]. Silver is widely used in different industries especially the electronics industry, due to its highest electrical conductivity [3], outstanding thermal conductivities [4] and the lowest electrical resistivity among all metals. The plating process might produce massive wastewater containing silver ions. Therefore, silver removal and recovery from the plating wastewater is necessary and urgent, not only for water conservation and silver recycling, but also for improving the economic efficiency of enterprises [5].

There are several methods used for the Ag(I) removal and recovery, including extraction using cyanide solution [6] or nitric acid [3], ion-exchange [7], reverse osmosis [8] and adsorption [9]. However, these methods can cause further environmental problems, such as the generation of waste acid solutions [6] and toxic fumes [10]. Some studies have considered the conversion of Ag(I) to insoluble precipitates like AgCl or Ag_2SO_4 [11]. But the process of reducing AgCl or Ag_2SO_4 to silver metal is complicated and energy-consuming [12]. Adsorption was believed as a competitive technique for Ag(I) removal at low concentration, considering its low cost, simple operation, and high efficiency. Up to now, various adsorbents including active carbon [13], fly ash [9], expanded perlite [14], biosorbents [15] and electrospun [16] have been designed and prepared. Nevertheless, these traditional adsorbents

* Corresponding author at: Beijing Key Laboratory of Functional Materials for Building Structure and Environment Remediation, Beijing University of Civil Engineering and Architecture, Beijing 100044, China.
E-mail address: wangchongchen@bucea.edu.cn (C.-C. Wang).

https://doi.org/10.1016/j.cej.2022.136306
Received 4 January 2022; Received in revised form 12 March 2022; Accepted 6 April 2022
Available online 10 April 2022

generally suffered from some disadvantages like lower adsorption capacity as well as poor reusability and stability [17]. Thus, it is imperative to develop new adsorbent materials to overcome the above shortcomings.

Metal-organic frameworks (MOFs) were an emerging family of porous crystalline solids with intrinsic porosity, in which the metals or metal-oxo clusters are bonded by organic linkers [18]. Up to now, MOFs are extensively utilized in numerous research fields like gas storage [19], adsorption/separation [20], water treatment [21], fluorescent sensing [22], drug delivery [23]. MOFs demonstrate some unique adsorption properties, owing to the combination of hydrophilic [24] and hydrophobic molecules [25] in the framework.

Up to now, some MOFs based adsorbents have been assessed for the adsorption to silver ions [26–28]. Zhang et al. synthesized a fluorescent MOF FITC@BTPY-NH_2 to achieve selective sensing detect and adsorptive removal of Ag(I) in aqueous solution [26]. Ding et al. designed and synthesized two types of new rhodanine (Rd)-functionalized UiO-66 adsorbents, with maximum Ag(I) uptake capacities of 112 and 163 $mg{\cdot}g^{-1}$ [27]. Bastian Moll et al. tuned UiO-66 with mercaptoacetic acid (HMAc) for accomplishing a maximum capacity for Ag(I) of > 84 $mg{\cdot}g^{-1}$ [28].

Within this work, NH_2-MIL-125 was adopted as adsorbent to capture Ag(I) from the simulated wastewater considering that its metal-carboxylate bonding, large surface area and tunable structure could provide extra binding sites to interact with Ag(I). The adsorption behaviors of the NH_2-MIL-125 toward Ag(I) were clarified, in which the adsorption mechanisms were further explored from both the experimental findings and the DFT calculations. Considering the reuse of the high cost NH_2-MIL-125 the Ag(I) saturated NH_2-MIL-125 was either desorbed for adsorbent re-generation or calcined to produce Ag doped TiO_2 catalyst for organic pollutants degradation (Scheme 1). From these points, the 3Rs (reduce, recycle and reuse) approach was practiced in this works, to accomplish that one stone killed three birds, i.e. pollutant elimination, resource recovery and resource utilization.

2. Experimental

All information of the chemicals and reagents, analytical methods and instruments are provided in the Supplementary Information (SI).

2.1. Synthesis of NH_2-MIL-125(Ti) and MIL-125(Ti)

The NH_2-MIL-125 particles were produced according to the previous report [29]. 2-Aminoterephthalic acid (2.2 g) was completely dissolved in 36.0 mL N,N-dimethylformamide (DMF). The mixture of 4.0 mL Me-OH (methanol) and 2.4 mL tetrabutyl titanate was added into the above-stated solution. The obtained matrix was transferred into a 100.0 mL Teflon-lined stainless steel autoclave, which was reacted at 150℃ for 48 h. The solid products were collected by centrifugation (8000 rpm) after cooling down to room temperature (25℃), which were washed with 200 mL DMF and Me-OH, respectively. The final products were activated at 80 °C under vacuum for 12 h.

The synthesis of MIL-125 was identical to that of NH_2-MIL-125 except for replacing 2-aminoterephthalic acid with 1,4-benzendicarboxylic acid.

2.2. Adsorption experiments

Within this work, the adsorption behaviors of NH_2-MIL-125 particles toward cationic Ag(I) were investigated through batch adsorption tests. The $AgNO_3$ was dissolved into ultra-pure water to obtain the aqueous Ag (I) solution, and the solution pH values were adjusted by 1.0 M HNO_3 or NaOH solution. The kinetics investigations were carried out by adding 20.0 mg NH_2-MIL-125 particles into 100 mL Ag(I) solution with concentrations ranging from 5.0 to 100.0 $mg{\cdot}L^{-1}$ at pH being 6.0, which was stirred for 2 h at 170 rpm under 298 K. The adsorption isotherms were studied by incubating NH_2-MIL-125 particles with Ag(I) solution under the temperature of 293 K, 298 K and 303 K, respectively.

During the sorption process, 2.5 mL sample was regularly drawn from the treated solution by 0.22 μm springe filters. The residual Ag(I) concentrations in aqueous solution were determined by ICP-OES (ICP-500, Focused Photonics Inc). The adsorption ability of NH_2-MIL-125 was calculated by Eq. (1).

$$q = \frac{(C_0 - C_e)V}{m} \tag{1}$$

Where, C_0 and C_e ($mg{\cdot}L^{-1}$) represented Ag(I) concentrations at initial and equilibrium, respectively; V and m are the liquid phase volume (L) and adsorbent mass (g), respectively.

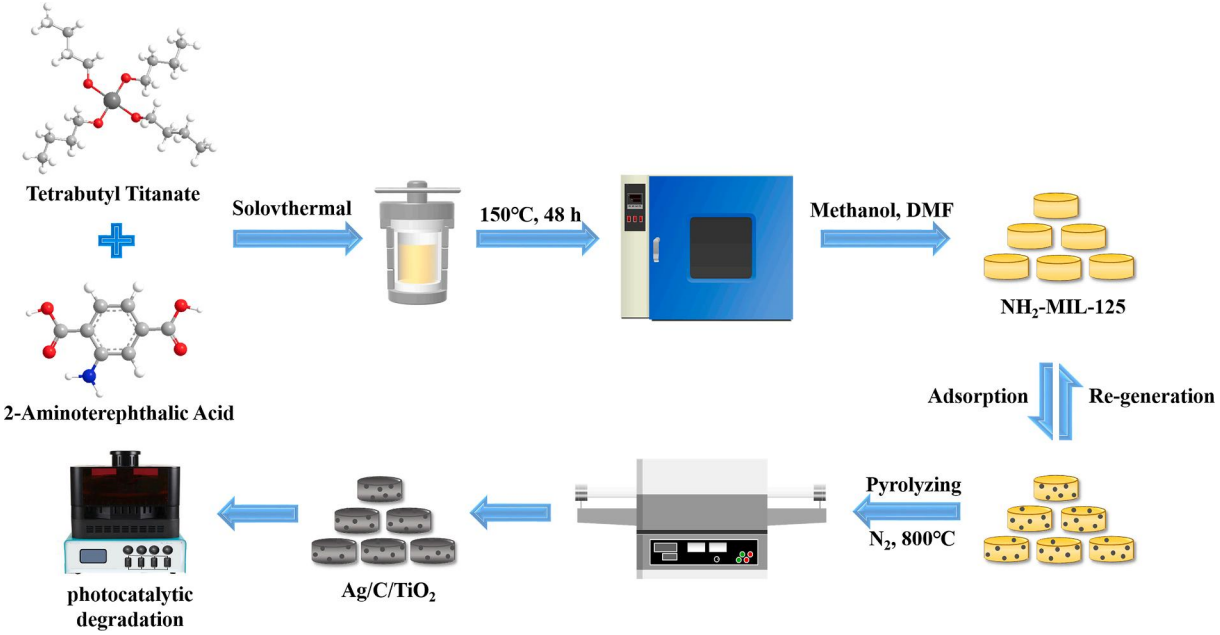

Scheme 1. Synthetic illustration for the NH_2-MIL-125 preparation and the 3Rs approach.

2.3. Fixed-bed breakthrough column study

It was generally difficult to conduct fixed-bed breakthrough test adopting NH_2-MIL-125 particles to fill the column due to that the close packing of the fine particles can block the fluid flow. To overcome this difficulty, the fine particles was immobilized on cotton fibers, which was further packed into column to carry out breakthrough test [30]. Detailly, 0.5 g as-prepared NH_2-MIL-125 particles and 1.0 g cotton fiber were mixed and stirred in a beaker containing 100 mL pure water for 12 h with a magnetic stirrer to obtain NH_2-MIL-125/Cotton (NC). The obtained NC was dried at 333 K in an oven. The fixed-bed adsorption test was performed by filling 7.0 g NC (the immobilized NH_2-MIL-125 particles being 700.0 mg) in a column to fabricate a fixed bed of 10 cm height and 5.7 cm^2 cross sectional area (Fig. 5a). Through this fixed bed, the aqueous Ag(I) solution passed downward at a flow rate of 4.0 $mL{\cdot}min^{-1}$. During the sorption, 2.5 mL sample was collected regularly to determine the residual Ag(I) concentrations with the aid of ICP-OES.

3. Results and discussion

3.1. Characterizations of NH_2-MIL-125

The PXRD patterns of NH_2-MIL-125 and MIL-125 particles fitted perfectly with the simulated PXRD patterns obtained from the single crystal data (CCDC 751175) (Fig. 1a), implying that both NH_2-MIL-125 and MIL-125 were successfully synthesized. The NH_2-MIL-125 exhibited higher water stability under different pH values than MIL-125 (Fig. S1), which can be ascribed to the amino functional groups and its function of altering the water sorption property [31]. The SEM images of MIL-125 and NH_2-MIL-125 particles were illustrated in Fig. 1c and d, in which both the NH_2-MIL-125 and MIL-125 exhibited as smooth regular discs with particle size of ca. 500 nm. As illustrated in Fig. 1b and Fig. S2a, the NH_2-MIL-125 and MIL-125 displayed the BET surface areas of 1250 $m^2{\cdot}g^{-1}$ and 1469 $m^2{\cdot}g^{-1}$, with pore volumes of 0.59 $cm^3{\cdot}g^{-1}$ and 0.65 $cm^3{\cdot}g^{-1}$, respectively, which were similar to the previous reports [32].

3.2. Adsorption performance

3.2.1. Adsorption isotherms

It was observed that both NH_2-MIL-125 and MIL-125 displayed good sorption activities toward Ag(I) cations (Fig. 2a). The maximum sorption capacities of NH_2-MIL-125 and MIL-125 were 192.51 $mg{\cdot}g^{-1}$ and 139.83 $mg{\cdot}g^{-1}$, which were superior to the previous counterpart adsorbents (Table S1 and Fig. S2b). The $–NH_2$ groups in the NH_2-MIL-125 might contribute to the higher adsorption performance due to the interaction between Ag(I) and nitrogen atoms in $–NH_2$ group [33].

Three adsorption isotherm models like Langmuir, Freundlich and Dubinin-Radushkevich (D-R) were selected to investigate how the Ag(I) ions interact with the NH_2-MIL-125 (Eqs. S1-S3). As depicted in Fig. 2b, Fig. S3 and Table 1, the higher fitting coefficients R^2 ranging from 0.9831 to 0.9932 of langmuir equation indicated that the uptake of Ag(I) by NH_2-MIL-125 adsorbent can be described well by the Langmuir equation [34]. The maximum sorption capacity q_{max} (192.3 $mg{\cdot}g^{-1}$) calculated by the Langmuir model at 293 K was similar to the corresponding experimental data (192.51 $mg{\cdot}g^{-1}$). The calculated q_{max} from the Langmuir model decreased with the temperature, demonstrating that the adsorption of Ag(I) ions over NH_2-MIL-125 is exothermic.

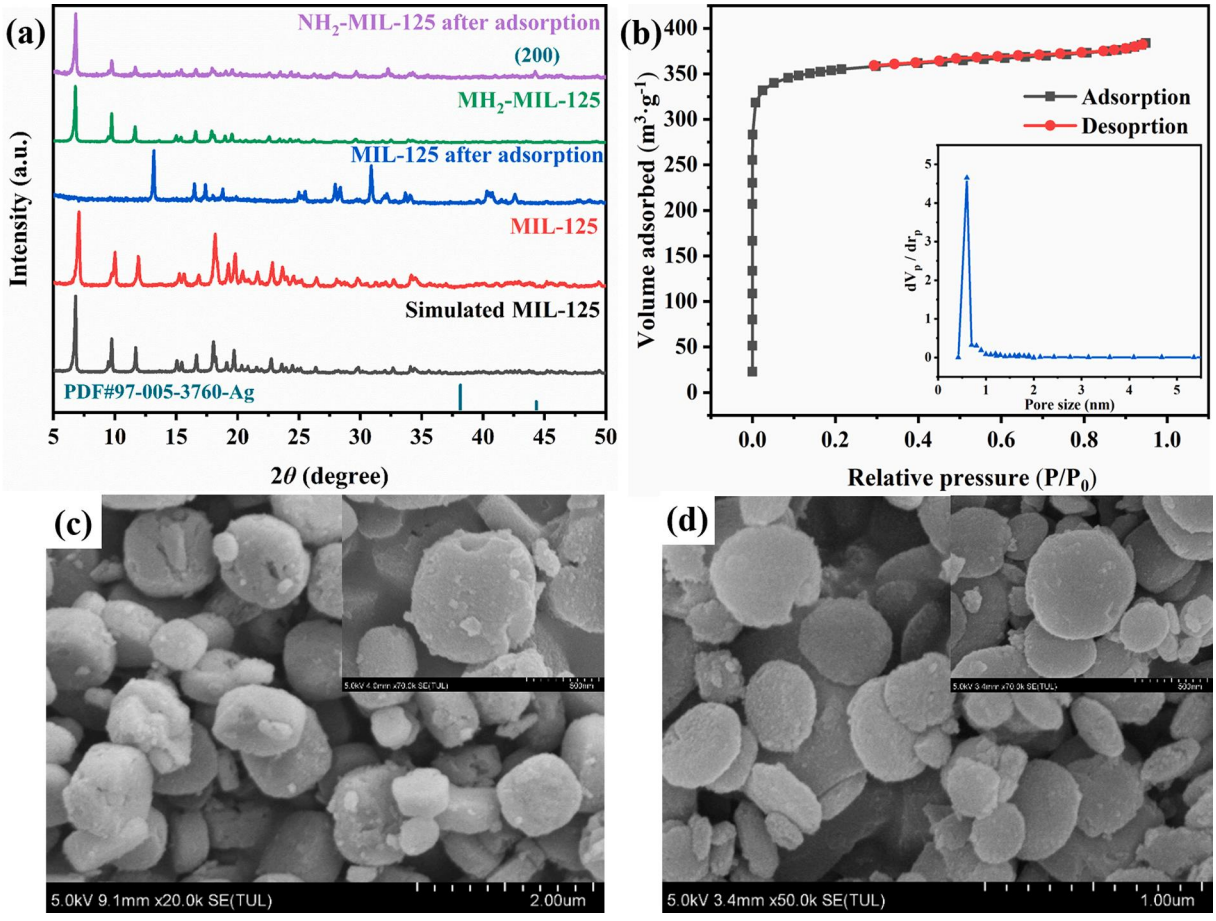

Fig. 1. (a) The PXRD patterns of MIL-125 and NH_2-MIL-125 before and after adsorption; (b) the isotherms of N_2 adsorption–desorption and the pore width distribution curve for NH_2-MIL-125; the SEM images of (c) MIL-125 and (d) NH_2-MIL-125.

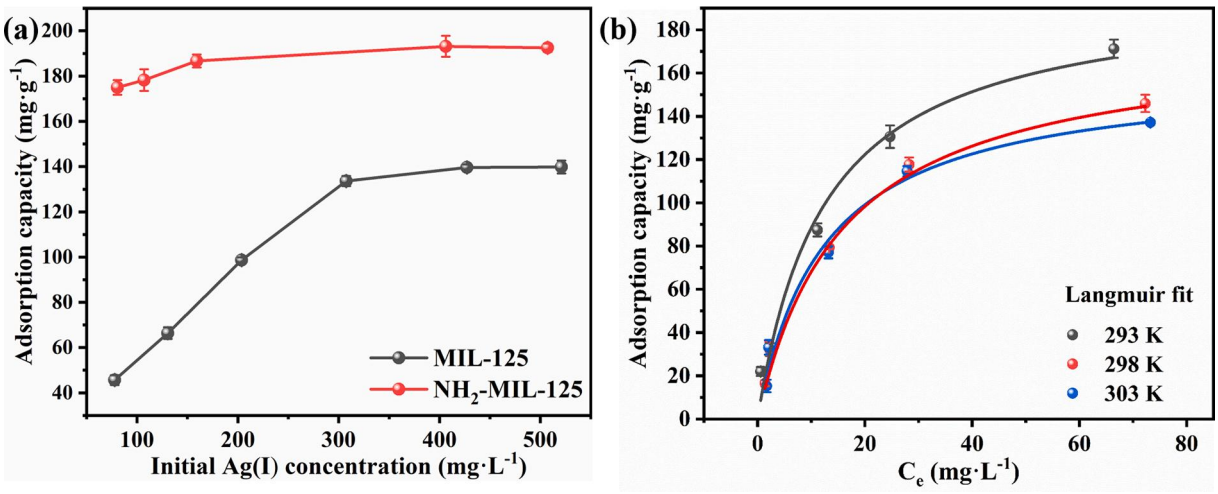

Fig. 2. (a) The maximum adsorption capacities of MIL-125 and NH_2-MIL-125; (b) the Langmuir fitting of NH_2-MIL-125 for Ag(I) adsorption under different temperatures. (Experimental conditions: sorbent dose = 0.2 mg·mL^{-1}, initial pH = 5.6).

Table 1
The constants of Langmuir, Freundlich and D-R for Ag(I) adsorption by NH_2-MIL-125 at different temperatures.

T/K	Langmuir			Freundlich			D-R		
	K_L (L·min^{-1})	q_m (mg·g^{-1})	R^2	K_f (mg·g^{-1})	1/n	R^2	K_{DR}	E (kJ·mol^{-1})	R^2
293	0.1008	192.307	0.9831	26.4353	0.4644	0.9799	0.0002	50	0.8691
298	0.0828	163.934	0.9932	16.9811	0.5457	0.9546	0.00009	75	0.8114
303	0.0808	161.290	0.9898	16.7987	0.5413	0.9118	0.00008	79	0.8147

3.2.2. *Thermodynamic parameters*

The thermodynamic parameters like enthalpy change (ΔH^o, kJ·mol^{-1}), entropy change (ΔS^o, J·mol^{-1}·K^{-1}) as well as Gibbs free energy change (ΔG^o, kJ·mol^{-1}) were calculated by Eqs. S4-5 based on the results obtained from the Langmuir adsorption isotherm to further clarify the sorption behaviors. As listed in Table 2, the nagetive ΔH^o (-16.30 kJ·mol^{-1}) indicated the exothermic sorption process. It can be found that the increasing temperature inhibited the adsorption process [13], which was affirmed by the q_{max} obtained at lower temperature. The positive ΔS^o (21.58 J·mol^{-1}·K^{-1}) implied that the the high affinity of NH_2-MIL-125 towards Ag(I) ions led to the increase of the randomness [35], which might be related to the production of some new species (the Ag^0 element in this work) on the adsorbent surface during the adsorption process [36]. The Gibbs free energy changes (ΔG^o) from –22.46 to –22.67 kJ·mol^{-1} at the temperatures ranging from 293 K to 303 K further verfiried that the uptake of Ag(I) onto NH_2-MIL-125 was thermodynamically spontaneous. Also, all the nagetive ΔH^o, the increasing ΔG^o with decreasing temperture and the decreasing K_L in the Langmuir model with increasing temperature can jointly affirmed that relatvely low temperature was favorable to the Ag(I) ions adsorption onto NH_2-MIL-125 adsorbent.

3.2.3. *Adsorption kinetics*

The adsorption kinetics like pseudo-first-order model and pseudo-second-order model were adopted to explore the sorption process of Ag(I) on NH_2-MIL-125 and MIL-125 [37]. The kinetic parameters of these two models were calculated from the fitting results following Eqs. S6-9 (Fig. 3a, Fig. S4a, Table 3 and Table S2). For both NH_2-MIL-125 and MIL-125, the high calculated R^2 values (>0.999) of the pseudo-second-order model at different Ag(I) concentrations demonstrated that the sorption process could be preferedlly described by the pseudo-second-order model rather than the pseudo-first-order one [38]. As well, the calculated equilibrium adsorption capacities (q_e) under different initial concentrations were close to the corresponding experimental q_e values, further affirming the satisfied agreement with the pseudo-second-order model. It can be proposed that the adsorption processes of Ag(I) on the surface of both NH_2-MIL-125 and MIL-125 involved the chemical adsorption.

Table 2
The thermodynamic parameters of the sorption processes of Ag(I) over NH_2-MIL-125.

ΔS^o (J·mol^{-1}·K^{-1})	ΔH^o (kJ·mol^{-1})	R^2	ΔG^o (kJ·mol^{-1})		
21.58	−16.30	0.98	293 K	298 K	303 K
			−22.46	−22.49	−22.67

According to the intra-particle diffusion model, the step that determines the adsorption rate could be contributed to the diffusion of adsorbent particles into the pores of the adsorbent [39]. As presented in Fig. 3b and Fig. S4b, the plots displayed two line patterns, demonstrating that the adsorption of Ag(I) on NH_2-MIL-125 and MIL-125 were accomplished via two stages. The 1st stage demonstrated that the mass transfer of Ag(I) ions occurred between the aqueous solution and the boundary layer of the adsorbents via film diffusion [40]. The 2nd stage implied that the Ag(I) ions could be sorbed into the pore surface of the MOF adsorbents via the pore diffusion process [41]. The intra-particle diffusion constants K_I and K_{II} for the corresponding 1st and 2nd stage were listed in Table 3 and Table S2. From the results of $K_I > K_{II}$, it was implied that the Ag(I) ions diffused rapidly among the NH_2-MIL-125 particles in the beginning of the sorption process, and then the intra-particle diffusion process slowed down [42]. Similar findings were observed in the adsorption kinetics of MIL-125. It was revealed that the adsorption kinetics of the Ag(I) ions onto both NH_2-MIL-125 and MIL-125 could be jointly controlled by both film diffusion and intraparticle diffusion.

3.3. *Influencing factors*

In general, the increase of the sorbent dosage decrease the ratio of adsorbent ions to adsorbent active sites, which could increase the

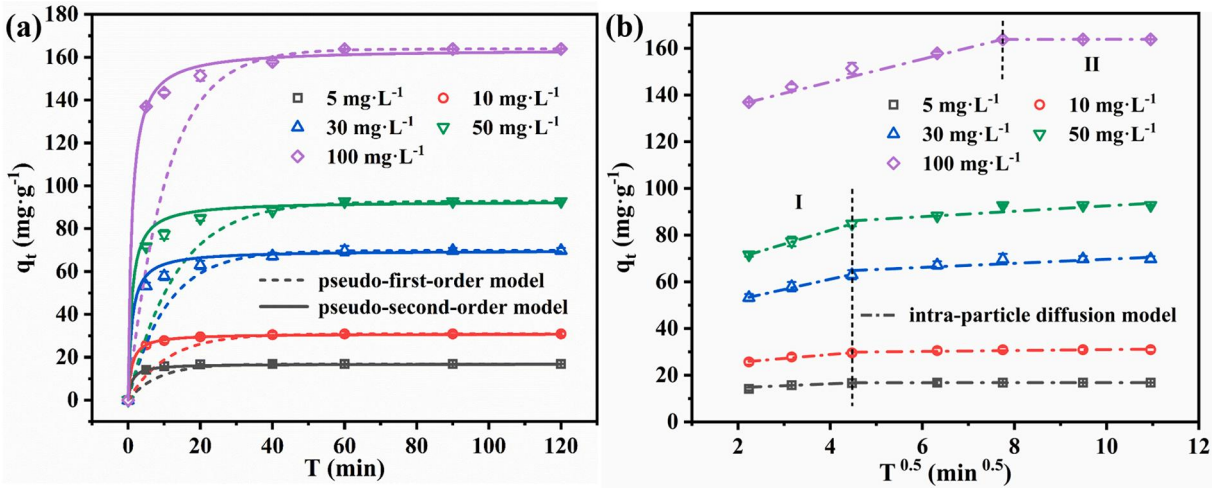

Fig. 3. (a) The pseudo-first-order, pseudo-second-order kinetics, and (b) intra-particle diffusion models for sorption process of NH_2-MIL-125 towards Ag(I). (Experimental conditions: sorbent dose = 0.2 mg·mL^{-1}, initial pH = 5.6, T = 25℃).

Table 3
Kinetic parameter of Ag(I) adsorption with different concentrations onto NH_2-MIL-125 (298 K).

Model	parameter	5 mg·g^{-1}	10 mg·g^{-1}	30 mg·g^{-1}	50 mg·g^{-1}	100 mg·g^{-1}
Pseudo-first-order	k_1	0.03	0.09	0.09	0.09	0.10
	q_e (mg·g^{-1})	0.72	2.49	3.86	3.96	4.37
	R^2	0.6053	0.9868	0.9703	0.9539	0.9508
Pseudo-second-order	k_2	0.06	0.03	0.01	0.01	0.01
	q_e (mg·g^{-1})	16.95	31.15	70.92	94.34	166.67
	R^2	0.9999	0.9999	0.9997	0.9996	0.9998
Intra-particle diffusion	K_I	0.82	1.64	4.38	5.90	5.37
	K_{II}	0.01	0.20	0.88	1.16	0.02
Experimental q_e (mg·g^{-1})		16.86	30.95	69.81	92.78	163.86

adsorption efficiency [43]. As illustrated in Fig. 4a, the Ag(I) ions emilination efficiencies increased steeply from 22.5% to 68.1% with the increasing NH_2-MIL-125 dosage from 100 mg·L^{-1} to 500 mg·L^{-1}, due to that the increasing NH_2-MIL-125 dosage could provide more active sites to accomplish higher ratio of active sites to Ag(I). However, the increasing MIL-125 dosage led to slow increasing Ag(I) removal efficiecy, possibly due to that the higher dosages of MIL-125 adsorbent lead to aggregation of adsorbent particles and reduction of available empty sites [44].

The pH values is another critical parameter affecting the sorption performance of adsorbents [45]. The pH effect on the adsorption process is mainly due to the changes in the zeta potential of the adsorbents and the state of presence of the adsorbate [46,47]. Considering that Ag(I) could be precipitated under even weakly alkaline conditions, the pH range of the Ag(I) solution (50 mg·L^{-1}) was adjusted between 2.0 and 6.0. As shown in Fig. 4b, the Ag(I) adsorptive removal efficiecies of both MIL-125 and NH_2-MIL-125 increased as the pH increased from 2.0 to 6.0. In addition, the Ag(I) sorption capacity over NH_2-MIL-125 was better than MIL-125 under various pH values. As depicted in Fig. 4d, the surfaces of NH_2-MIL-125 and MIL-125 were negatively charged as pH > 2.5 and pH > 4.5, respectively. Therefore, the cationic Ag(I) ions were easily attracted to the negatively charged NH_2-MIL-125 and MIL-125 by electrostatic attraction. As pH = 6, the electronegativity of the adsorbents were the strongest, thus the maximum adsorption efficiency was obtained at pH being 6.0.

Generally, there are different competing cations like Cu(II), Zn(II), and Fe(III) presenting in silver plating wastewater [3]. To explore the impact of coexistence cations toward the removal efficiencies of NH_2-MIL-125, series experiments were designed to simulate silver plating wastewater samples like binary (Ag/Cu, Ag/Zn and Ag/Fe) and multivariate (Ag/Cu/Zn/Fe) systems [48]. As shown in Fig. 4c, the Cu(II), Zn (II), and Fe(III) exerted insignificant inlfluence on the adsorption activity of NH_2-MIL-125 as adsorbent, indicating that NH_2-MIL-125 can accompish selective and efficient uptake toward Ag(I) in simulated silver plating wastewater.

To evaluate the adsorption selectivity of NH_2-MIL-125, the adsorption efficiencies toward the four heavy metals (Ag(I), Cu(II), Zn(II), and Fe(III)) under competitive conditions were illustrated in Fig. S5. Clearly, NH_2-MIL-125 exhibited a certain selectivity toward silver ions, in which the obtained adsorption ability followed the order of Ag(I) > Cu(II) > Fe (III) > Zn(II). The affinities of different binding sites on NH_2-MIL-125 toward the four ions were assessed via DFT calculations. As shown in Fig. S6 and Table S3, adsorption energies (E_{ads}) and bond distances [49] were used as the parameters to quantify the affinity of the metal ion to the binding sites. The calculated E_{ads} values for heavy metals located at oxygen atoms within the core of the Ti-O cluster were remarkably higher than those of nitrogen atom on amino group. The Ag-O bond exhibited the shorter bond distance (1.930, 2.472 and 2.560 Å) than those of Cu–O, Fe-O and Zn-O. As well, the E_{ads} of Ag-O bond was thus much higher than those of the other three M−O bonds. These DFT calculations were consistent with the experimental adsorption results, indicating that NH_2-MIL-125 demonstrated the selective adsorption toward Ag(I) ions.

3.4. Fixed-bed column experiments

The fixed-bed column is widely used in large-scale industrial wastewater treatment due to its simplicity of operation and continuous control [50]. Thus, for the purpose of treating silver plating wastewater in large quantities on industrial scale, the cotton fiber was chosen as the carrier for the immobilized NH_2-MIL-125 (NH_2-MIL-125@Cotton, being named NC) to pack the fixed bed column (Fig. 5a), in which the treated aqueous solution was distributed evenly over the adsorbent in the fixed

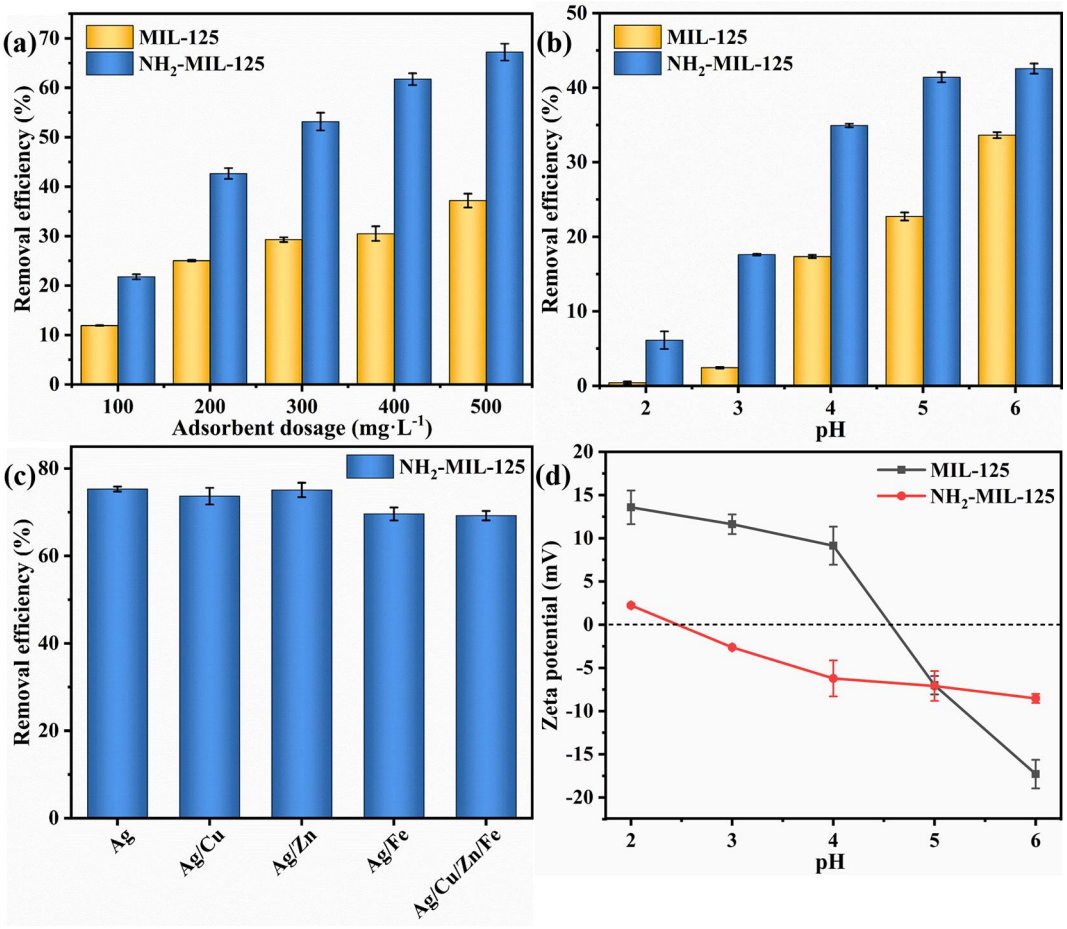

Fig. 4. The sorption capacities of MIL-125 and NH_2-MIL-125 at (a) different adsorbent dosages (0.1–0.5 mg·mL^{-1}); (b) different pH (C_0 = 50 mg·L^{-1}) (c) Removal efficiencies of NH_2-MIL-125 for Ag ions in the single, binary, and multivariate solutions (Experimental conditions: sorbent dose = 0.2 mg·mL^{-1}, initial pH = 5.6, [Ag (I)] = 2 mg·L^{-1}, [Cu(II)] = 0.5 mg·L^{-1}, [Zn(II)] = 0.5 mg·L^{-1}, [Fe(III)] = 0.5 mg·L^{-1}); and (d) the zeta potential under different pHs.

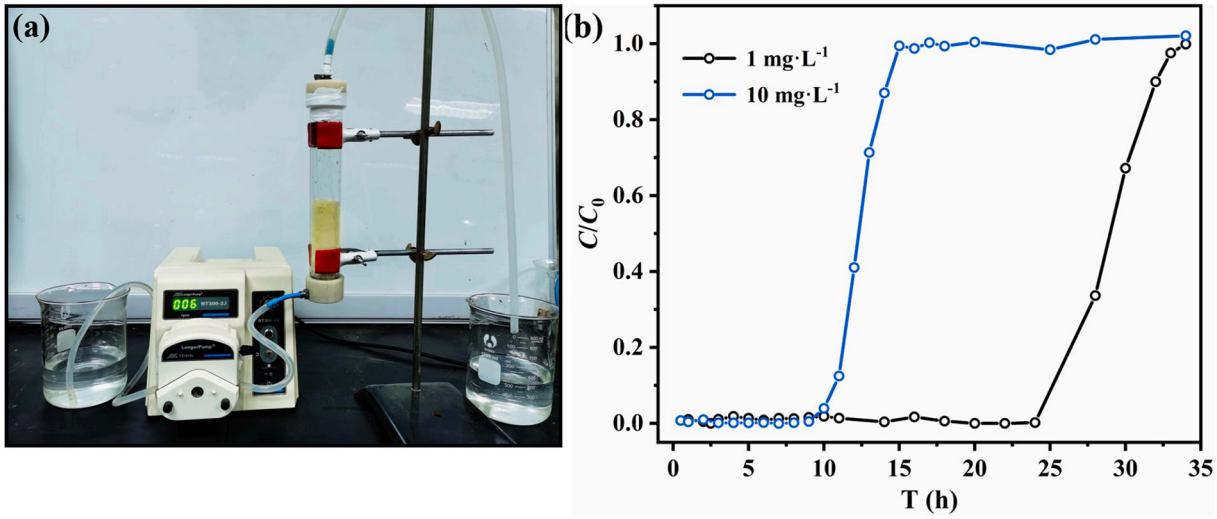

Fig. 5. (a) The picture of fixed-bed column setup and (b) the breakthrough curve of adsorption process over NH_2-MIL-125 towards Ag(I). (Experimental conditions: initial pH = 5.6, T = 25℃, flow rate = 4 mL·min^{-1}).

bed was constant [51]. As illustrated in Fig. S7, the individual cotton fibers exhibited negligible adsorption capacity for silver ions.

As shown in Fig. 5b, Ag(I) could be efficiently trapped with a removal efficiency > 98% within 8 h during the continous adsorption process over the fixed-bed column, in which the Ag(I) concentration in the effluent decreased to the level of 0.001–0.01 mg·L^{-1} with the influent aqueous solution containing Ag(I) of 10.0 mg·L^{-1}. The corresponding treatment time could be increased to 24 h as the concentration of the Ag (I) solution was reduced to 1 ppm. After reaching adsorption saturation, the breakthrough curve increased sharply due to the exist of the mass

transfer zone (MTZ) [52].

3.5. Adsorption mechanism

In the PXRD patterns of NH_2-MIL-125 after adsorption (Fig. 1a), the peak at $2\theta = 46.1^\circ$ corresponds to the typical peak of crystalline silver (JCPDS No. 04–0783) [53], implying that Ag(I) ions might be reduced into Ag^0 element via the reaction between the $–NH_2$ groups of NH_2-MIL-125 and Ag(I) [54]. In contrast, the PXRD patterns of MIL-125 after Ag (I) adsorption were quite different from the pristine MIL-125, indicating that obvious composition and phrase changes happened.

From the FTIR spectra of the NH_2-MIL-125 and MIL-125 before and after adsorption in Fig. 6a, it was observed that the –OH vibration peaks of NH_2-MIL-125 and MIL-125 moved from 3424 cm^{-1} and 3414 cm^{-1} to 3457 cm^{-1} and 3462 cm^{-1}, respectively, which may be assiciated with the complexation of Ag(I) to –OH. For NH_2-MIL-125, the specific peak representing the stretching vibration of C-N at 1261 cm^{-1} was shifted to 1256 cm^{-1} after adsorpiton. While, the bending vibration of the N–H bond was altered from 1640 cm^{-1} to 1625 cm^{-1}, due to that the the amino group participated the reduction reaction from Ag(I) to Ag^0 [55]. All the FTIR information indicated that the Ag(I) ions in the aqueous solution might interact with the N and O atoms in NH_2-MIL-125 [54]. The elemental mapping in the energy-dispersive X-ray (EDS) images from Fig. 6b also confirmed the presence of O, Ti, N and Ag elements in the used NH_2-MIL-125 (Fig. 6b).

To further elaborate the sorption mechanism of Ag(I) onto adsorbent NH_2-MIL-125, the X-ray photoelectron spectroscopy (XPS) determinations was performed. As for the overall XPS spectra of the NH_2-MIL-125 and MIL-125 after Ag(I) adsorption (Fig. 7a), the peaks at 285.7, 368.7, 400.1, 458.8, and 532.3 eV were assigned to C 1 s, Ag 3d, N 1 s, Ti 3d and O 1 s, respectively, in which the peaks of 368.7 eV (Ag 3d) implied the retention of silver on the adsorbents. In the high-resolution O 1 s spectrum of pristine NH_2-MIL-125 (Fig. 7b), three peaks located at 532.40, 531.77 and 530.20 eV are assigned to the O atoms in C=O, –OH, as well as Ti-oxo clusters, respectively [54,56]. After adsorption of Ag(I), the area ratios of C=O (532.40 eV) and –OH (531.77 eV) decreased from 25% and 48% to 24% and 14%, implying that the oxygen atoms in C=O and hydroxyl were involved in the Ag(I) adsorption processes [57]. In addition, the intensity of Ti-O peak decreased, and the Ag-O peak appeared after adsorption. These results indicate that silver would form Ag-O coordination by exchange the C=O, hydroxyl groups and Ti-oxo clusters of NH_2-MIL-125 in the sorption process. As depicted in Fig. 7c, a new peak of Ag-N located at 400.7 eV presented after adsorption [58]. The decrease of the proportion (from 28% to 4%) of peak of -N-$^+$ (402.99 eV) and the increase (from 72% to 83%) of the peak of –NH=$^+$ (399.47 eV) occurred after the Ag(I) uptake [54], implying Ag-N interaction formed between the N and Ag atoms, which can be contributed to the superior sorption performance of NH_2-MIL-125 to MIL-125. It was observed that Ag^0 element formed over the two adsorbents after Ag(I) uptake, which can be affirmed by the observations of XPS peaks at 368.73 and 374.88 eV of NH_2-MIL-125 as well as the peaks at 368.67 eV and 374.87 eV of MIL-125 [59]. It was implied that partial silver ions adsorbed over the adsorbents were reduced to metallic silver. Lu et al also reported that the electron donor groups like hydroxyl could reduce Ag(I) to Ag^0 in the aqueous solution [60].

The high-resolution TEM (HRTEM) revealed that the Ag^0 NPs were dispered on the NH_2-MIL-125 (Fig. 8a), in which the lattice fringe ca. 0.235 nm corresponding to the (1 1 1) facet of Ag^0 was observed (Fig. 8**b**) [61]. The selected-area electron diffraction (SAED) image demonstrated that the most distinct and vital diffraction patterns can also be allocated the (1 1 1), (2 2 0) and (3 1 1) plane of Ag^0 in the NH_2-MIL-125 after Ag(I) adsorption [62]. The EIS Nyquist plots (Fig. 8c) indicated that the arc radii of the NH_2-MIL-125 and MIL-125 adsorbents after adsorption are much smaller than those of pristine ones. The Ag^0 nanoparticles on the surface of the NH_2-MIL-125 and MIL-125 adsorbents improved the conductivity of the adsorbents due to its good conductivity. Generally, the smaller radius implied the faster charge transfer, the lower interfacial resistance and better electrical conductivity [63].

Also, the density functional theory (DFT) calculation were employed to profoundly understand the adsorption mechanism of NH_2-MIL-125 towards Ag(I) ions. It was proposed that the silver ion could be adsorbed onto six possible binding sites of NH_2-MIL-125, in which the corresponding adsorption energies (E_{ads}) [64] and net amount of electron transfer [65] were calculated. As illustrated in Fig. 9a, the carbon, hydrogen, oxygen, nitrogen, titanium, silver atoms of NH_2-MIL-125 were labelled as brown, white, red, gray, blue and argent, respectively. According to the calculations, it was clear that all the binding sites on the NH_2-MIL-125 could efficiently intereact with Ag(I) in aqueous media. The No. 1 to No. 6 sites in Fig. 9b indicated that Ag (the argent ball represented silver atoms) ions were coordinated to oxygen atoms on the carbon–oxygen double bond as well as hydroxyl group, nitrogen atom on amino group, oxygen atoms in the periphery of the Ti-O cluster core, transverse and longitudinal oxygen atoms within the core of the Ti-O cluster, respectively. The E_{ads} at sites from No. 1 to No. 6 were −0.755, −0.257, −0.433, −0.583, −1.621 and −1.051 eV, respectively. The negative values of E_{ads} indicated the adsorption process was an exothermic processes. In general, the larger absolute value of E_{ads} represented the stronger interaction between adsorbent and adsorbate as well as the more stable adsorption conformation [66,67]. The net amount of electrons transfers in the No. 5 sites (0.943 electron charge)

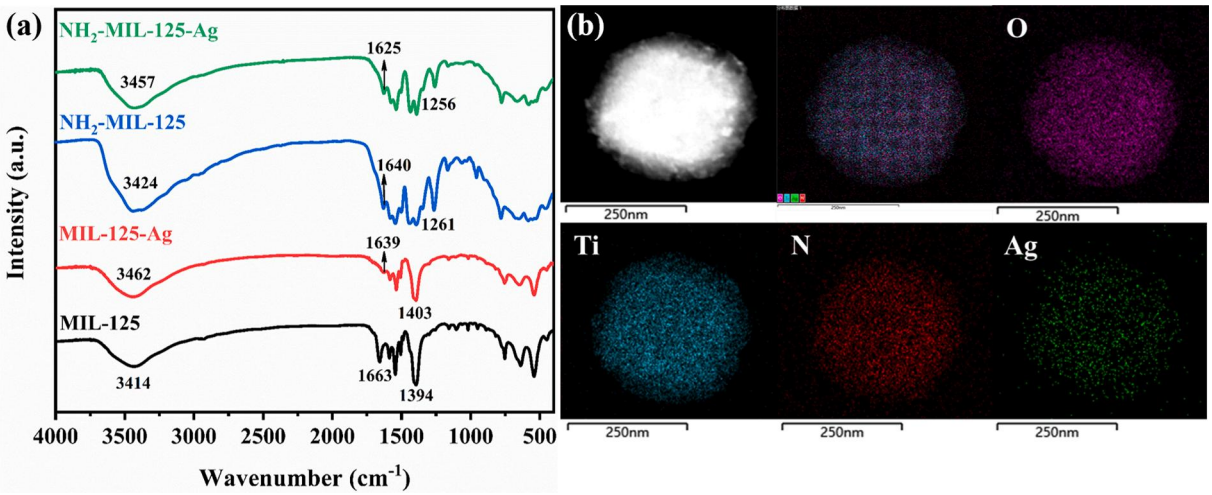

Fig. 6. (a) The FTIR spectra of the pristine and used MIL-125 and NH_2-MIL-125; (b) The EDS mapping of NH_2-MIL-125 after adsorption.

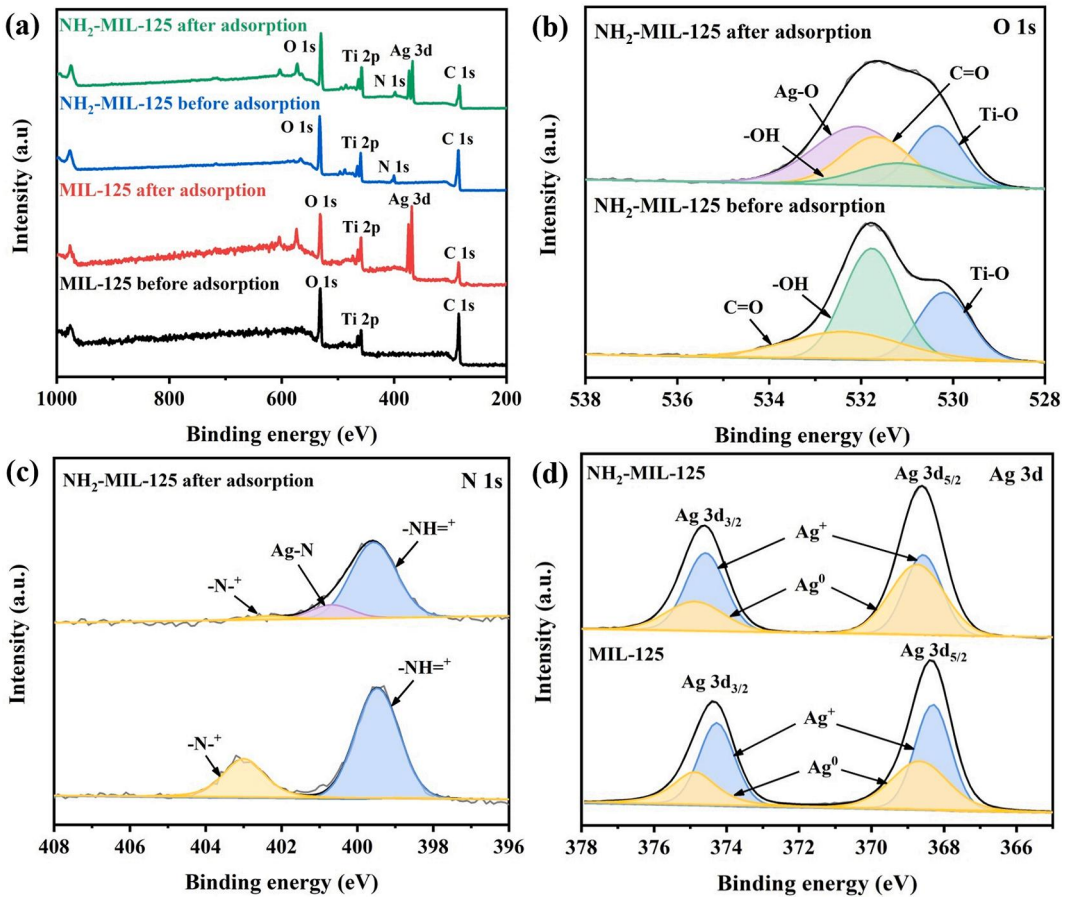

Fig. 7. The XPS spectra of the pristine and the used MIL-125 and NH_2-MIL-125, (a)Survey, (b) O 1 s, (c) N 3d; (d) Ag 3d.

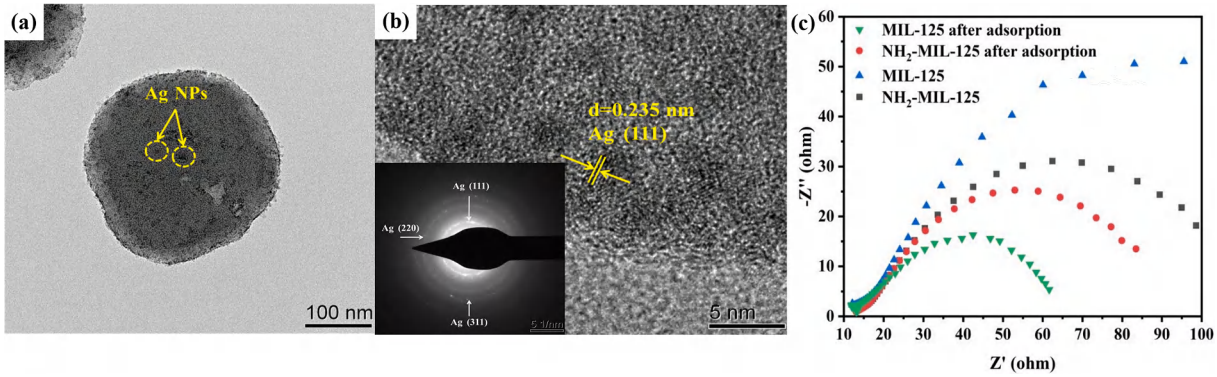

Fig. 8. (a) TEM, (b) High-resolution TEM, SAED pattern (inset) of NH_2-MIL-125 after adsorption, (c) EIS of adsorbents before and after adsorption.

was more than those in the other sites (0.715, 0.370, 0.482, 0.708 and 0.917 electron charge for No. 1–4 and No. 6, respectively). Thus, for all the six selected sites, the affinities toward Ag of the corresponding sites were in the order of 5 > 6 > 1 > 4 > 3 > 2, in which the metal binding at No. 5 site was deemed as the most stable conformation.

Being judged from both the experimental findings and the DFT calculation results, it was concluded that the coordinative interactions between nitrogen or oxygen atoms of NH_2-MIL-125 and silver along with the electrostatic interactions were probable adsorption mechanisms (Scheme 2).

3.6. Subsequent disposal of the used NH_2-MIL-125

The Ag(I) adsorbed onto the NH_2-MIL-125 can be mostly desorbed by 1% HNO_3, indicating that NH_2-MIL-125 adsorbent with unchanged morphology can be regenerated and reused (Fig. S8 and Fig. S9). To practice 3Rs (reduce, recycle and reuse) approach, we proposed to treat the used NH_2-MIL-125 into Ag^0-loaded TiO_2 photocatalyst. It was well known that Ag NPs loaded TiO_2 will display the improved photocatalysis activity due to that the Ag NPs could heavily inhibited the recombination of the photo-generated e^-/h^+ pairs [68–70]. Nevertheless, Ag/TiO_2 obtained by pre-synthesized metal NPs decorated on the surface of TiO_2 with the aggregation of metal NPs on the surface of TiO_2, which may reduce the photocatalytic efficiency [71]. In this study, the preparation method of chemical methods could effectively eliminate this drawback. Besides, the XPS spectra of Ag/C/TiO_2 in Fig. S10 revealed the presence of carbon, which could benefit the efficient separation of photo-induced e^-/h^+ pairs [72]. The Ag/C/TiO_2 was obtained from the used NH_2-MIL-

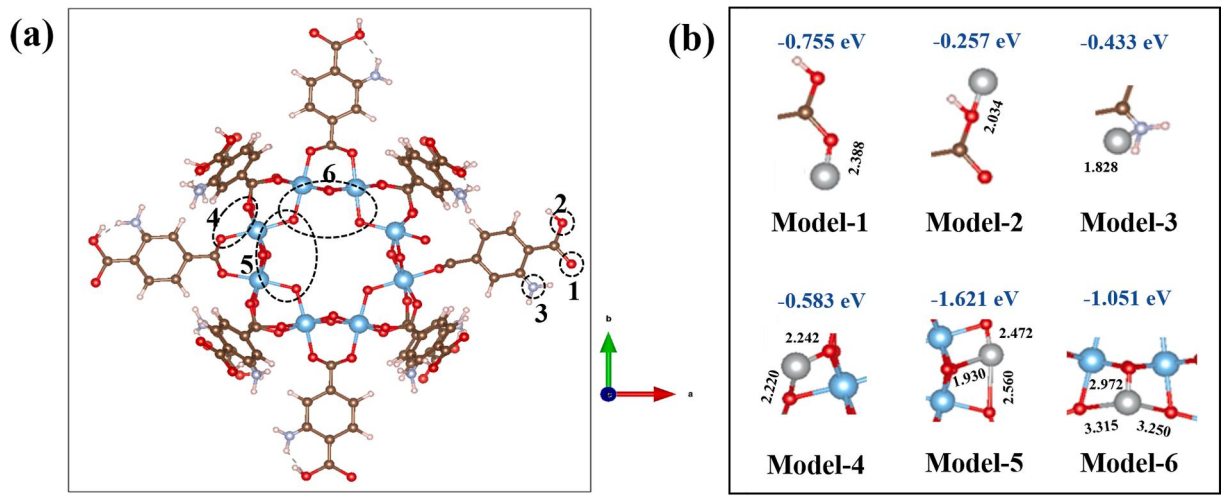

Fig. 9. (a) Structural diagram of NH_2-MIL-125 and (b) its six selected representative binding sites. The brown, white, red, gray, blue and argent sphere represents C, H, O, N, Ti and Ag atom, respectively.

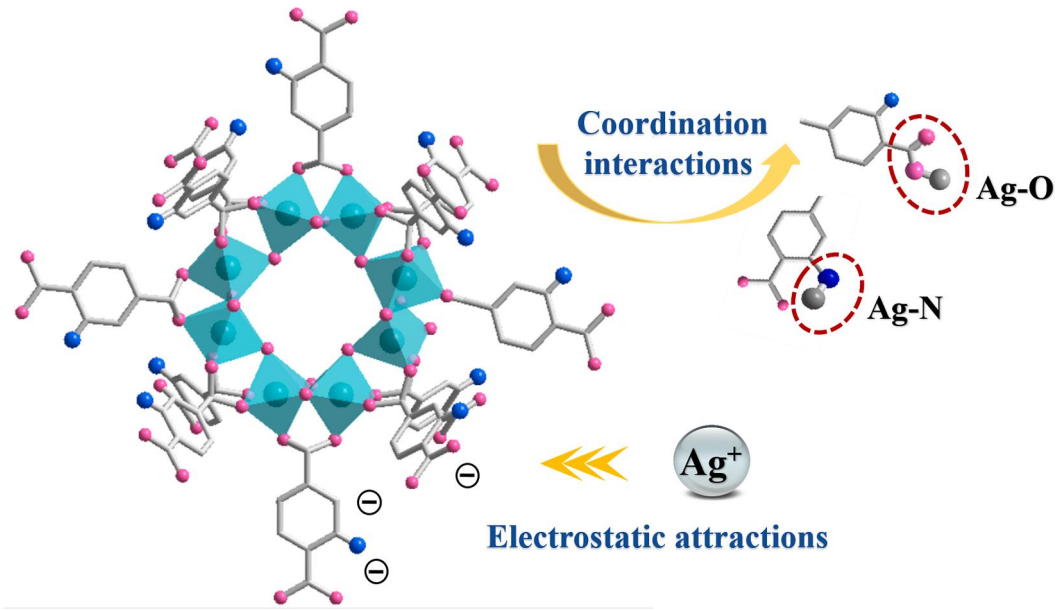

Scheme 2. Adsorption mechanism of NH_2-MIL-125 for Ag(I).

125 adsorbent via thermally treatment at 800 °C under N_2 comdition, which could be applied to environment remediation with the advantages of simple preparation and low cost [73]. The PXRD peaks at 38.1°, 44.3°, 25.3°, 48.1°, 27.5°, 36.1° and 41.3° were indexed to the (111) and (200) crystal planes of Ag (PDF#97–005-3760), the (101), (200) crystal facets of anatase phase TiO_2 (PDF#97–002-4276) [74] as well as (110), (101), (111) crystal planes of rutile TiO_2 (PDF#97–002-3697) [75]. The HRTEM observation indicated that the as-synthetic Ag/C/TiO_2 maitained the morphology of NH_2-MIL-125 with particle size ca. 300 nm (inset of Fig. 10b), in which the lattice fringes of 0.324 nm and 0.235 nm corresponded to the (110) facet of the rutile TiO_2 and Ag^0 NPs, respectively [76].

The UV–vis DRS spectrum of the as-prepared Ag/C/TiO_2 indicated that it can be excited by the light with different wavelengthes (Fig. 10c). The E_g values (band gap energy) of the NH_2-MIL-125 before and after Ag (I) adsorption, Ag/C/TiO_2, C/TiO_2 (which was obtained by treating the pristine NH_2-MIL-125 thermally), TiO_2 (Degussa, P-25) were calculated (Eq. S10) to be 2.69, 2.56, 0.91, 2.37 and 3.39 eV, respectively (Fig. S11). Obviously, the band gap of Ag/C/TiO_2 was narrower than that of the C/TiO_2 nanoparticles, which is ascribed to the synergistic effect of the presence of carbon and Ag^0 nanoparticles [77]. The photocatalysis degradation activities of the obtained Ag/C/TiO_2 toward MB (methylene blue) as the typical organic pollutant model were measured under UV and visible light illumination. As depicted in Fig. 10d, the Ag/C/TiO_2 displayed better degradation performance by visible light illumination than that under UV light. Meanwhile, Ag/C/TiO_2 with the addition of Ag^0 exhibited better degradation performance than C/TiO_2 under the same condition (Fig. S13).

Especially, the introduction of H_2O_2 as hole scavenger significantly improved the degradation efficiency toward MB, in which > 90% MB can be degraded within 80 min (Fig. 10d). Some similar materials in previous studies had also shown dye degradation [78]. In addition, the apparent rate constant (k_{obs}) was calculated using pseudo-first-order model to further evaluate the MB degradation performance of Ag/C/TiO_2. The k_{obs} of Ag/C/TiO_2/H_2O_2 system toward MB degradation was 0.0457 min^{-1} (Fig. S14), which was higher than those of other systems. As shown in Fig. S15, the introduction of tertiary butyl alcohol (TBA), L-histidine and oxalic acid significantly inhibited the MB degradation

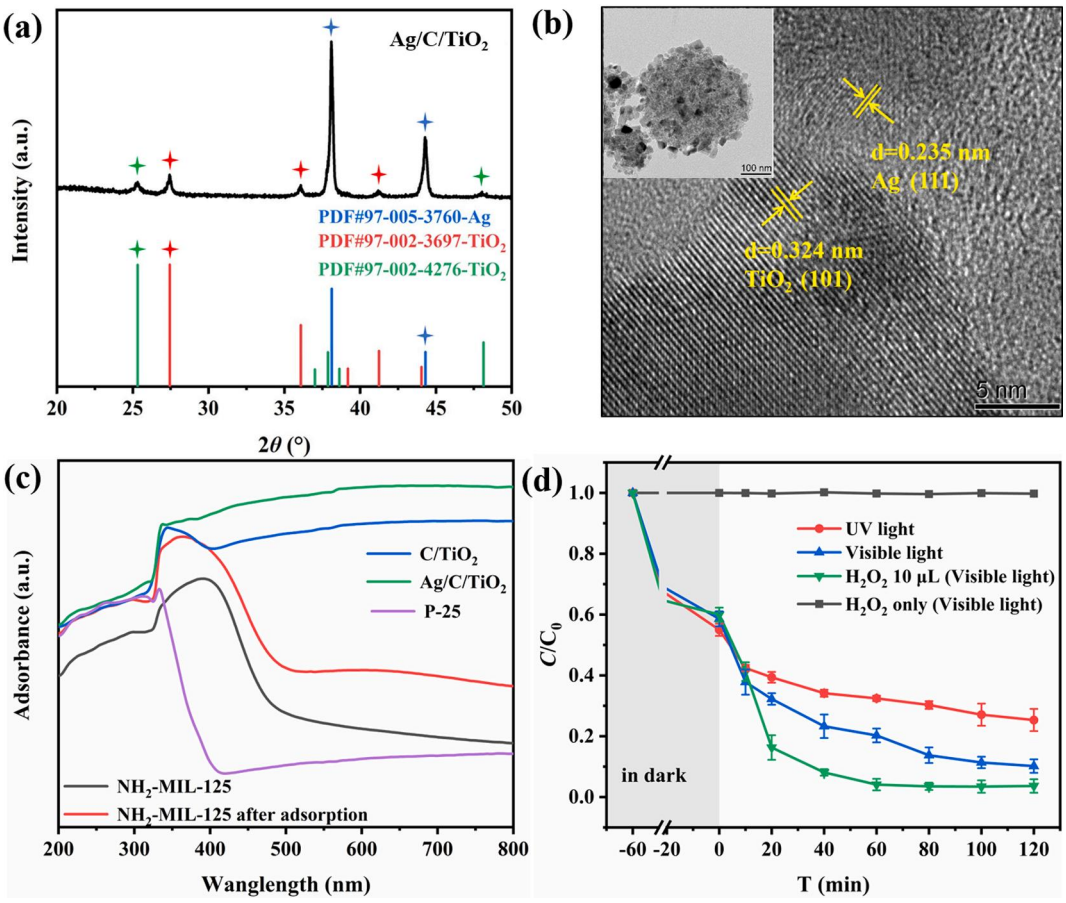

Fig. 10. (a) The PXRD patterns, (b) High-resolution TEM, (c) UV–Vis DRS and (d) the MB degradation under different conditions. (Experimental conditions: dose = 0.2 mg·mL^{-1}, initial pH = 5.9, $[MB]_0$ = 10 mg·L^{-1}, H_2O_2 dose = 10.0 μL).

efficiency, implying that the ·OH radicals, non-radical $^1O_2$ and holes (h^+) were active species. The recyclability of Ag/C/TiO_2 was investigated by successive reusability tests (Fig. S16). It can be seen that the MB degradation efficiency could reach 90% within 90 min after three cycles, revealing the relatively high recyclability. The structure of Ag/C/TiO_2 was not changed obviously after three cycles of catalytic experiments (Fig. S17), implying its good stability and reusability. Similarly, Ag/C/TiO_2 exhibited a certain photocatalytic degradation performance towards phenol (Fig. S18).

Also, our previous work demonstrated that the TiO_2 NPs produced from MIL-125 can accomplish effective benzene degradation upon the visible light [79], implying that the used NH_2-MIL-125 might be treated to produce powerful doped TiO_2 NPs photocatalyst.

4. Conclusion

In all, NH_2-MIL-125 was applied to accomplish the adsorptive removal of Ag(I) from the simulated silver-plating wastewater. The NH_2-MIL-125 displayed satisfactory stability, good selectivity and maximum adsorption capacity, which was superior to most reported counterpart adsorbents. The dominant interactions of the sorption process were contributed to the electrostatic attraction along with the coordination interactions between NH_2-MIL-125 and Ag(I) cations. The fixed-bed column experiments demonstrated that NH_2-MIL-125 could be the prospective candidate for large-scale Ag(I) removal from wastewater. Based on the 3Rs (reduce, recycle and reuse) approach, the Ag(I) saturated NH_2-MIL-125 was thermally treated into Ag/C/TiO_2 photocatalyst to accomplish organic pollutant elimination. This work aimed to remove the Ag(I) in the wastewater via effective NH_2-MIL-125 and to reuse the used adsorbent for obtaining high added value photocatalyst, providing an approach of combination of pollutant reduction, resource recycle and environmental materials reuse.

Declaration of Competing Interest

The authors declare that they have no known competing financial interests or personal relationships that could have appeared to influence the work reported in this paper.

Acknowledgments

This work was supported by National Natural Science Foundation of China (51878023), Beijing Talent Project (2020A27), Science and Technology General Project of Beijing Municipal Education Commission (KM202110016010), The Fundamental Research Funds for Beijing University of Civil Engineering and Architecture (X20147/X20141/X20135/X20146), Young Teachers' Research Ability Enhancement Program for Beijing University of Civil Engineering and Architecture (X21085) and BUCEA Post Graduate Innovation Project (2021).

Appendix A. Supplementary data

Supplementary data to this article can be found online at https://doi.org/10.1016/j.cej.2022.136306.

References

[1] J. Yang, B. Hou, J. Wang, B. Tian, J. Bi, N. Wang, X. Li, X. Huang, Nanomaterials for the removal of heavy metals from wastewater, Nanomaterials 9 (2019) 424.
[2] A. Güvenç, B. Karabacakolu, Use of electrodialysis to remove silver ions frommodel solutions and wastewater, Desalination 172 (1) (2005) 7–17.

[3] J.-N. Gu, J. Liang, C. Chen, K. Li, W. Zhou, J. Jia, T. Sun, Treatment of real deplating wastewater through an environmental friendly precipitation-electrodeposition-oxidation process: Recovery of silver and copper and reuse of wastewater, Sep. Purif. Technol. 248 (2020), 117082.

[4] Y. Gao, Y. Zhou, H. Wang, W. Lin, Y. Wang, D. Sun, J. Hong, Q. Li, Simultaneous Silver Recovery and Cyanide Removal from Electroplating Wastewater by Pulse Current Electrolysis Using Static Cylinder Electrodes, Ind. Eng. Chem. Res. 52 (17) (2013) 5871–5879.

[5] Y. Chen, M. Xu, J. Wen, Y.u. Wan, Q. Zhao, X. Cao, Y. Ding, Z.L. Wang, H. Li, Z. Bian, Selective recovery of precious metals through photocatalysis, Nat. Sustain. 4 (7) (2021) 618–626.

[6] K. Folens, S. Huysman, S. Van Hulle, G. Du Laing, Chemical and economic optimization of the coagulation-flocculation process for silver removal and recovery from industrial wastewater, Sep. Purif. Technol. 179 (2017) 145–151.

[7] S. Çoruh, G. Şenel, O.N. Ergun, A comparison of the properties of natural clinoptilolites and their ion-exchange capacities for silver removal, J. Hazard. Mater. 180 (1-3) (2010) 486–492.

[8] C.S. Slater, R.C. Ahlert, C.G. Uchrin, Applications of reverse osmosis to complex industrial wastewater treatment, Desalination 48 (2) (1983) 171–187.

[9] C. Mu, L. Zhang, X. Zhang, L. Zhong, Y. Li, Selective adsorption of Ag (I) from aqueous solutions using Chitosan/polydopamine@ C@ magnetic fly ash adsorbent beads, J. Hazard. Mater. 381 (2020), 120943.

[10] Z. Sheng, Y. Liu, Effects of silver nanoparticles on wastewater biofilms, Water Res. 45 (18) (2011) 6039–6050.

[11] S. Syed, Silver recovery aqueous techniques from diverse sources: Hydrometallurgy in recycling, Waste Manag. 50 (2016) 234–256.

[12] A. Bas, E. Yazici, H. Deveci, Recovery of silver from X-ray film processing effluents by hydrogen peroxide treatment, Hydrometallurgy 121 (2012) 22–27.

[13] N.M. Mahmoodi, M. Taghizadeh, A. Taghizadeh, Mesoporous activated carbons of low-cost agricultural bio-wastes with high adsorption capacity: preparation and artificial neural network modeling of dye removal from single and multicomponent (binary and ternary) systems, J. Mol. Liq. 269 (2018) 217–228.

[14] H. Ghassabzadeh, A. Mohadespour, M. Torab-Mostaedi, P. Zaheri, M.G. Maragheh, H. Taheri, Adsorption of Ag, Cu and Hg from aqueous solutions using expanded perlite, J. Hazard. Mater. 177 (1-3) (2010) 950–955.

[15] Y. Zhao, D. Wang, H. Xie, S.W. Won, L. Cui, G. Wu, Adsorption of Ag (I) from aqueous solution by waste yeast: kinetic, equilibrium and mechanism studies, Bioprocess Biosyst. Eng. 38 (1) (2015) 69–77.

[16] S.A. Hosseini, M. Vossoughi, N.M. Mahmoodi, M. Sadrzadeh, Efficient dye removal from aqueous solution by high-performance electrospun nanofibrous membranes through incorporation of SiO_2 nanoparticles, J. Clean. Prod. 183 (2018) 1197–1206.

[17] J. Li, X. Wang, G. Zhao, C. Chen, Z. Chai, A. Alsaedi, T. Hayat, X. Wang, Metal–organic framework-based materials: superior adsorbents for the capture of toxic and radioactive metal ions, Chem. Soc. Rev. 47 (2018) 2322–2356.

[18] C.-C. Wang, X.-H. Yi, P. Wang, Powerful combination of MOFs and C_3N_4 for enhanced photocatalytic performance, Appl. Catal. B 247 (2019) 24–48.

[19] Y. Hu, Z. Liu, J. Xu, Y. Huang, Y. Song, Evidence of pressure enhanced CO_2 storage in ZIF-8 probed by FTIR spectroscopy, J. Am. Chem. Soc. 135 (25) (2013) 9287–9290.

[20] I. Ahmed, S.H. Jhung, Applications of metal-organic frameworks in adsorption/separation processes via hydrogen bonding interactions, Chem. Eng. J. 310 (2017) 197–215.

[21] N.M. Mahmoodi, M. Oveisi, A. Taghizadeh, M. Taghizadeh, Synthesis of pearl necklace-like ZIF-8@ chitosan/PVA nanofiber with synergistic effect for recycling aqueous dye removal, Carbohydr. Polym. 227 (2020), 115364.

[22] C.-Y. Wang, C.-C. Wang, X.-W. Zhang, X.-Y. Ren, B. Yu, P. Wang, Z.-X. Zhao, H. Fu, A new Eu-MOF for ratiometrically fluorescent detection toward quinolone antibiotics and selective detection toward tetracycline antibiotics, Chinese Chemical Letters 33 (3) (2022) 1353–1357.

[23] I. Abánades Lázaro, S. Haddad, J.M. Rodrigo-Muñoz, R.J. Marshall, B. Sastre, V. del Pozo, D. Fairen-Jimenez, R.S. Forgan, Surface-functionalization of Zr-fumarate MOF for selective cytotoxicity and immune system compatibility in nanoscale drug delivery, ACS Appl, Mater. Interfaces 10 (37) (2018) 31146–31157.

[24] L. Zhang, Y. Li, Y. Wang, S. Ma, J. Ou, Y. Shen, M. Ye, H. Uyama, Integration of covalent organic frameworks into hydrophilic membrane with hierarchical porous structure for fast adsorption of metal ions, J. Hazard. Mater. 407 (2021), 124390.

[25] M.I.H. Mohideen, B.o. Xiao, P.S. Wheatley, A.C. McKinlay, Y. Li, A.M.Z. Slawin, D. W. Aldous, N.F. Cessford, T. Düren, X. Zhao, R. Gill, K.M. Thomas, J.M. Griffin, S. E. Ashbrook, R.E. Morris, Protecting group and switchable pore-discriminating adsorption properties of a hydrophilic-hydrophobic metal-organic framework, Nat. Chem. 3 (4) (2011) 304–310.

[26] L. Zhang, Y. Jian, J. Wang, C. He, X. Li, T. Liu, C. Duan, Post-modification of a MOF through a fluorescent-labeling technology for the selective sensing and adsorption of Ag^+ in aqueous solution, Dalton Trans. 41 (2012) 10153–10155.

[27] L. Ding, P. Shao, Y. Luo, X. Yin, S. Yu, L. Fang, L. Yang, J. Yang, X. Luo, Functionalization of UiO-66-NH_2 with rhodanine via amidation: Towarding a robust adsorbent with dual coordination sites for selective capture of Ag (I) from wastewater, Chem. Eng. J. 382 (2020), 123009.

[28] B. Moll, T. Müller, C. Schlüsener, A. Schmitz, P. Brandt, S. Öztürk, C. Janiak, Modulated synthesis of thiol-functionalized fcu and hcp UiO-66 (Zr) for the removal of silver (i) ions from water, Mater. Adv. 2 (2021) 804–812.

[29] H. Wang, X. Yuan, Y. Wu, G. Zeng, X. Chen, L. Leng, Z. Wu, L. Jiang, H. Li, Facile synthesis of amino-functionalized titanium metal-organic frameworks and their superior visible-light photocatalytic activity for Cr(VI) reduction, J. Hazard. Mater. 286 (2015) 187–194.

[30] D. Pang, C.-C. Wang, P. Wang, W. Liu, H. Fu, C. Zhao, Superior removal of inorganic and organic arsenic pollutants from water with MIL-88A (Fe) decorated on cotton fibers, Chemosphere 254 (2020), 126829.

[31] F. Jeremias, V. Lozan, S.K. Henninger, C. Janiak, Programming MOFs for water sorption: amino-functionalized MIL-125 and UiO-66 for heat transformation and heat storage applications, Dalton Trans. 42 (2013) 15967–15973.

[32] S.-N. Kim, J. Kim, H.-Y. Kim, H.-Y. Cho, W.-S. Ahn, Adsorption/catalytic properties of MIL-125 and NH_2-MIL-125, Catal. Today 204 (2013) 85–93.

[33] M. Wang, R. Qu, C. Sun, P. Yin, H. Chen, Dynamic adsorption behavior and mechanism of transition metal ions on silica gels functionalized with hydroxyl-or amino-terminated polyamines, Chem. Eng. J. 221 (2013) 264–274.

[34] J. Chen, J. Ouyang, W. Chen, Z. Zheng, Z. Yang, Z. Liu, L. Zhou, Fabrication and adsorption mechanism of chitosan/Zr-MOF (UiO-66) composite foams for efficient removal of ketoprofen from aqueous solution, Chem. Eng. J. 431 (2022), 134045.

[35] J. Zhao, C. Wang, S. Wang, L. Zhang, B. Zhang, Selective recovery of Au (III) from wastewater by a recyclable magnetic $Ni_{0.6}Fe_{2.4}O_4$ nanoparticels with mercaptothiadiazole: Interaction models and adsorption mechanisms, J. Clean. Prod. 236 (2019), 117605.

[36] B. Dash, B. Dash, S.S. Rath, A thorough understanding of the adsorption of Ni (II), Cd (II) and Zn (II) on goethite using experiments and molecular dynamics simulation, Sep. Purif. Technol. 240 (2020), 116649.

[37] Z. Aksu, Equilibrium and kinetic modelling of cadmium (II) biosorption by C. vulgaris in a batch system: effect of temperature, Sep. Purif. Technol. 21 (3) (2001) 285–294.

[38] M. Li, Y. Liu, F. Li, C. Shen, Y.V. Kaneti, Y. Yamauchi, B. Yuliarto, B. Chen, C.-C. Wang, Defect-rich hierarchical porous uio-66 (zr) for tunable phosphate removal, Environ. Sci. Technol. 55 (2021) 13209–13218.

[39] W.J. Weber, J.C. Morris, Kinetics of adsorption on carbon from solution, J. Sanit. Eng. Div. 89 (2) (1963) 31–59.

[40] R. Gupta, S.K. Gupta, D.D. Pathak, Selective adsorption of toxic heavy metal ions using guanine-functionalized mesoporous silica [SBA-16-g] from aqueous solution, Microporous Mesoporous Mater. 288 (2019), 109577.

[41] S. Dash, H. Chaudhuri, R. Gupta, U.G. Nair, A. Sarkar, Fabrication and application of low-cost thiol functionalized coal fly ash for selective adsorption of heavy toxic metal ions from water, Ind. Eng. Chem. Res. 56 (6) (2017) 1461–1470.

[42] K. Ahamad, R. Singh, I. Baruah, H. Choudhury, M. Sharma, Equilibrium and kinetics modeling of fluoride adsorption onto activated alumina, alum and brick powder, Groundw, Sustain. Dev. 7 (2018) 452–458.

[43] F. Ahmadijokani, S. Tajahmadi, A. Bahi, H. Molavi, M. Rezakazemi, F. Ko, T. M. Aminabhavi, M. Arjmand, Ethylenediamine-functionalized Zr-based MOF for efficient removal of heavy metal ions from water, Chemosphere 264 (2021), 128466.

[44] S. Naeimi, H. Faghihian, Performance of novel adsorbent prepared by magnetic metal-organic framework (MOF) modified by potassium nickel hexacyanoferrate for removal of Cs^+ from aqueous solution, Sep. Purif. Technol. 175 (2017) 255–265.

[45] C. Wang, G. Lin, J. Zhao, S. Wang, L. Zhang, Enhancing Au (III) adsorption capacity and selectivity via engineering MOF with mercapto-1, 3, 4-thiadiazole, Chem. Eng. J. 388 (2020), 124221.

[46] J. He, Y. Xu, W. Wang, B. Hu, Z. Wang, X. Yang, Y. Wang, L. Yang, Ce (III) nanocomposites by partial thermal decomposition of Ce-MOF for effective phosphate adsorption in a wide pH range, Chem. Eng. J. 379 (2020), 122431.

[47] X.-D. Du, C.-C. Wang, J.-G. Liu, X.-D. Zhao, J. Zhong, Y.-X. Li, J. Li, P. Wang, Extensive and selective adsorption of ZIF-67 towards organic dyes: performance and mechanism, J. Colloid Interface Sci. 506 (2017) 437–441.

[48] H. Chiu, K. Tsang, R. Lee, Treatment of electroplating wastes, J. Inst. Water Pollut. Control 86 (1987) 12–19.

[49] B. Tansel, Significance of thermodynamic and physical characteristics on permeation of ions during membrane separation: Hydrated radius, hydration free energy and viscous effects, Sep. Purif. Technol. 86 (2012) 119–126.

[50] G. Crini, E. Lichtfouse, L.D. Wilson, N. Morin-Crini, Conventional and non-conventional adsorbents for wastewater treatment, Environ. Chem. Lett. 17 (1) (2019) 195–213.

[51] X.-D. Du, C.-C. Wang, J. Zhong, J.-G. Liu, Y.-X. Li, P. Wang, Highly efficient removal of Pb^{2+} by a polyoxomolybdate-based organic-inorganic hybrid material $\{(4\text{-Hap})_4[Mo_8O_{26}]\}$, J. Environ. Chem. Eng. 5 (2) (2017) 1866–1873.

[52] M. Bhaumik, K. Setshedi, A. Maity, M.S. Onyango, Chromium (VI) removal from water using fixed bed column of polypyrrole/Fe_3O_4 nanocomposite, Sep. Purif. Technol. 110 (2013) 11–19.

[53] X. Wei, M. Luo, W. Li, L. Yang, X. Liang, L. Xu, P. Kong, H. Liu, Synthesis of silver nanoparticles by solar irradiation of cell-free Bacillus amyloliquefaciens extracts and $AgNO_3$, Bioresour. Technol. 103 (1) (2012) 273–278.

[54] W. Cui, J. Shang, H. Bai, J. Hu, D. Xu, J. Ding, W. Fan, W. Shi, In-situ implantation of plasmonic Ag into metal-organic frameworks for constructing efficient Ag/NH_2-MIL-125/TiO_2 photoanode, Chem. Eng. J. 388 (2020), 124206.

[55] Z. Chang, F. Li, X. Qi, B. Jiang, J. Kou, C. Sun, Selective and efficient adsorption of Au (III) in aqueous solution by Zr-based metal-organic frameworks (MOFs): An unconventional way for gold recycling, J. Hazard. Mater. 391 (2020), 122175.

[56] H. Guo, D.i. Guo, Z. Zheng, W. Weng, J. Chen, Visible-light photocatalytic activity of Ag@ MIL-125 (Ti) microspheres, Appl. Organomet. Chem. 29 (9) (2015) 618–623.

[57] J. Tang, J. Zhao, S. Wang, L. Zhang, M. Zhao, Z. Huang, Y. Hu, Pre-modification strategy to prepare a novel Zr-based MOF for selective adsorption of Palladium (II) from solution, Chem. Eng. J. 407 (2021), 127223.

[58] Y. He, L. Huang, Y. Zhao, W. Yang, T. Hao, B. Wu, H. Deng, D. Wei, H. Wang, J. Luo, A newly synthesized highly stable Ag/N-carbon electrode for enhanced

desalination by capacitive deionization, Environ. Sci, Nano 7 (10) (2020) 3007–3019.
[59] V. Muelas-Ramos, C. Belver, J. Rodriguez, J. Bedia, Synthesis of noble metal-decorated NH2-MIL-125 titanium MOF for the photocatalytic degradation of acetaminophen under solar irradiation, Sep. Purif. Technol. 272 (2021), 118896.
[60] Q. Lu, J. Deng, Y. Hou, H. Wang, H. Li, Y. Zhang, S. Yao, Hydroxyl-rich C-dots synthesized by a one-pot method and their application in the preparation of noble metal nanoparticles, Chem. Commun. (Camb.) 51 (33) (2015) 7164–7167.
[61] Y.X. Dong, X.L. Wang, E.M. Jin, S.M. Jeong, B. Jin, S.H. Lee, One-step hydrothermal synthesis of Ag decorated TiO_2 nanoparticles for dye-sensitized solar cell application, Renew, Energ. 135 (2019) 1207–1212.
[62] A. Celebioglu, F. Topuz, Z.I. Yildiz, T. Uyar, One-step green synthesis of antibacterial silver nanoparticles embedded in electrospun cyclodextrin nanofibers, Carbohydr. Polym. 207 (2019) 471–479.
[63] S.G. Khasevani, M. Taheri, M.R. Gholami, Green synthesis of Ag-Pt bimetallic nanoparticles supported on the Metal-Organic framework (MOF)–Derived metal oxides (γ-Fe_2O_3/CuO) nanocomposite as a reusable heterogeneous nanocatalyst and nanophotocatalyst, Mater. Chem. Phys. 261 (2021), 124218.
[64] J. Wang, C.-S. Cao, J. Wang, Y. Zhang, L. Zhu, Insights into highly efficient photodegradation of poly/perfluoroalkyl substances by In-MOF/BiOF heterojunctions: Built-in electric field and strong surface adsorption, Appl. Catal. B 304 (2022), 121013.
[65] P.J. Blowey, B. Sohail, L.A. Rochford, T. Lafosse, D.A. Duncan, P.T.P. Ryan, D. A. Warr, T.-L. Lee, G. Costantini, R.J. Maurer, D.P. Woodruff, Alkali doping leads to charge-transfer salt formation in a two-dimensional metal–organic framework, ACS Nano 14 (6) (2020) 7475–7483.
[66] S. Pandey, B. Demaske, O.A. Ejegbavwo, A.A. Berseneva, W. Setyawan, N. Shustova, S.R. Phillpot, Electronic structures and magnetism of Zr-, Th-, and U-based metal-organic frameworks (MOFs) by density functional theory, Comput. Mater. Sci. 184 (2020), 109903.
[67] C. Wang, C. Xiong, Y. He, C. Yang, X. Li, J. Zheng, S. Wang, Facile preparation of magnetic Zr-MOF for adsorption of Pb (II) and Cr (VI) from water: Adsorption characteristics and mechanisms, Chem. Eng. J. 415 (2021), 128923.
[68] Z. Jiang, W. Wei, D. Mao, C. Chen, Y. Shi, X. Lv, J. Xie, Silver-loaded nitrogen-doped yolk–shell mesoporous TiO_2 hollow microspheres with enhanced visible light photocatalytic activity, Nanoscale 7 (2) (2015) 784–797.
[69] N.M. Mahmoodi, A. Taghizadeh, M. Taghizadeh, J. Abdi, In situ deposition of Ag/AgCl on the surface of magnetic metal-organic framework nanocomposite and its application for the visible-light photocatalytic degradation of Rhodamine dye, J. Hazard. Mater. 378 (2019), 120741.
[70] K. Mohajershojaei, N.M. Mahmoodi, A. Khosravi, Immobilization of laccase enzyme onto titania nanoparticle and decolorization of dyes from single and binary systems, Biotechnol, Bioprocess Eng. 20 (1) (2015) 109–116.
[71] A. Kumar, P. Choudhary, A. Kumar, P.H. Camargo, V. Krishnan, Recent advances in plasmonic photocatalysis based on TiO_2 and noble metal nanoparticles for energy conversion, environmental remediation, and organic synthesis, Small 18 (2022) 2101638.
[72] X. Li, D. Wu, T. Hua, X. Lan, S. Han, J. Cheng, K.-S. Du, Y. Hu, Y. Chen, Micro/macrostructure and multicomponent design of catalysts by MOF-derived strategy: Opportunities for the application of nanomaterials-based advanced oxidation processes in wastewater treatment, Sci. Total Environ. 804 (2022), 150096.
[73] M. Oveisi, N.M. Mahmoodi, M.A. Asli, Facile and green synthesis of metal-organic framework/inorganic nanofiber using electrospinning for recyclable visible-light photocatalysis, J. Clean. Prod. 222 (2019) 669–684.
[74] Y. Ren, J. Zhang, Y. Liu, H. Li, H. Wei, B. Li, X. Wang, Synthesis and superior anode performances of TiO_2–carbon–rGO composites in lithium-ion batteries, ACS Appl. Mater. Interfaces 4 (9) (2012) 4776–4780.
[75] J. Li, X. Liu, Z. Sun, L. Pan, Novel Bi2MoO6/TiO2 heterostructure microspheres for degradation of benzene series compound under visible light irradiation, J. Colloid Interface Sci. 463 (2016) 145–153.
[76] J. Zeng, X. Liu, J. Wang, H. Lv, T. Zhu, Catalytic oxidation of benzene over MnOx/TiO2 catalysts and the mechanism study, J. Mol. Catal. A: Chem. 408 (2015) 221–227.
[77] L.-W. Zhang, H.-B. Fu, Y.-F. Zhu, Efficient TiO_2 photocatalysts from surface hybridization of TiO_2 particles with graphite-like carbon, Adv. Funct. Mater. 18 (15) (2008) 2180–2189.
[78] N.M. Mahmoodi, Photocatalytic degradation of dyes using carbon nanotube and titania nanoparticle, Water, Air, Soil Pollut. 224 (2013) 1–8.
[79] C. Zhao, Z. Wang, X.i. Chen, H. Chu, H. Fu, C.-C. Wang, Robust photocatalytic benzene degradation using mesoporous disk-like N-TiO_2 derived from MIL-125 (Ti), Chinese, J. Catal. 41 (8) (2020) 1186–1197.